4

Electronic Structure of Fluorinated Carbon Nanotubes

Maria Brzhezinskaya and Alexander Vinogradov
ALBA Synchrotron Light Source
Spain
Saint-Petersburg State University
Russia

1. Introduction

Chemical functionalization of carbon nanotubes (CNTs), i.e., attachment of individual atoms/molecules or their aggregates to CNTs, can extend the field of application of these nanosystems in nanoelectronics, sensorics, hydrogen power engineering, bioengineering, medicine, etc. (Dresselhaus & Dresselhaus, 2001; Burghard, 2005). In this respect, the fluorination of CNTs is of special interest because the fluorination results in a considerable decrease in the chemical inertness of the initial systems. Therefore, the fluorination is considered as a promising technological process for the first stage of the CNT chemical functionalization (Mickelson et al., 1998; Mickelson et al., 1999; Khabashesku et al., 2002; Lee, 2007). However, carbon materials react with fluorine over a wide range of external conditions. Consequently, the chemical composition, as well as the atomic and electronic structures of fluorinated carbon nanotubes (F-CNTs), depends substantially on the structure and properties of the initial materials and fluorination conditions, such as the reaction temperature and duration, the presence of catalysts, pressure, and concentration of fluorinating reactants (Touhara & Okino, 2000). All these factors need comprehensive investigations of fluorination products by different experimental methods.

Fitting of fluorination conditions that are necessary to perform the preset controllable restructuring of the CNT electronic structure remains at present the most topical problem of the carbon nanomaterial chemistry. Therefore, their atomic and electronic structures have been studied by using a limited number of experimental techniques. First and foremost, these are different microscopic techniques ensuring their visualization (Mickelson et al., 1998; Mickelson et al., 1999; Khabashesku et al., 2002; Lee, 2007; Touhara & Okino, 2000), Hamwi et al., 1997; Yudanov et. al., 2002; Hayashi et al., 2002; Lee et al., 2003), x-ray diffraction methods characterizing the degree of F-CNT crystallinity (Hamwi et al., 1997; Yudanov et. al., 2002) UV spectroscopy (Mickelson et al., 1999), Raman spectroscopy (Mickelson et al., 1998; Mickelson et al., 1999; Khabashesku et al., 2002; Lee, 2007; Touhara & Okino, 2000; Hamwi et al., 1997; Lee et al., 2003) and C 1*s* and F 1*s* core-level x-ray photoelectron spectroscopy (XPS) (Touhara & Okino, 2000; Hamwi et al., 1997; Lee et al., 2003; An et al, 2002) which provide information on the nature of chemical bonding between

carbon C and fluorine F atoms in F-CNTs. The investigations performed made it possible to determine the main conditions for the fluorination of single-walled carbon nanotubes (SWCNTs) and multi-walled carbon nanotubes (MWCNTs) to characterize their atomic structure and to obtain preliminary information on the specific features of their electronic structure due to the chemical bonding between C and F atoms. However, the data obtained in those works even with due regard for the results of the first theoretical calculations (Kudin et al., 2001; Park et al., 2003; Lebedev et al., 2003; Van Lier et al., 2005; Ewels et al., 2006) do not provide clear perception of the CNT fluorination mechanism and properties of fluorination products, which is necessary for expansion of practical use of F-CNTs.

Near-edge x-ray absorption fine-structure spectroscopy (NEXAFS) is at present one of the most efficient experimental methods (Stöhr, 1992; Chen, 1997). NEXAFS spectroscopy uses the relation between the spectral characteristics of the near-edge fine structure of x-ray absorption spectra and the parameters of the local atomic and electronic structures of the material under investigation in the vicinity of absorbing atoms. There are a few works in which NEXAFS spectroscopy has been successfully used to characterize pristine and oxidized CNTs (Kuznetsova et al., 2001; Tang et al., 2002; Schiessling et al., 2003; Banerjee et al., 2004; Banerjee et al., 2005; Hemray-Benny et al., 2006; Zhou et al., 2007). Total electron yield (TEY) mode is the most popular for recording of NEXAFS spectra (Gudat & Kunz, 1972). At the same time, TEY mode with probing depth approximately equal to the average MWCNT diameter (several tens of monolayers) does not allow one to get information about characteristics of investigated fluorinated multi-walled carbon nanotubes (F-MWCNTs) in their near-surface region where fluorination process can differ from that at greater depths. However, these data are of genuine fundamental interest and is indeed necessary for optimization of the MWCNT fluorination techniques. Such information for near-surface region only several graphene layers thick can be obtained, particularly, by XPS providing C 1*s* and F 1*s* core-level spectra of F-MWCNTs under investigation. XPS is an effective surface-sensitive method for investigation of material electronic structure (Huefner, 2003). In this case, the probing depth is adequate to the depth the registered electrons are emitted from, which depends on the electron kinetic energy. Therefore, the probing depth can vary from several tenth of nanometer (two to three atomic monolayers) to nanometers, depending on the energy of excitation photons. Presently, several works with XPS used to characterize fluorinated SWCNTs (F-SWCNTs) (Lee et al., 2007; Lee et al., 2003; An et al., 2002), fluorinated multiwalled nanoparticles (Okotrub et al., 2000), and F- CNTs (Shul'ga et al., 2007) are known.

In this chapter, the results of combined investigation of electronic structure of F-CNTs are presented. The high-resolution NEXAFS and XPS spectroscopies were used. The main goal of the present project is to elucidate the nature of chemical bonding between the carbon and fluorine atoms in the SWCNTs and MWCNTs, to evaluate a chemical state of fluorine and carbon atoms in these CNTs, to analyze modification of electronic structure of CNTs under fluorination, to characterize mechanism of CNT fluorination. The defluorination process of F-CNTs on thermal annealing has been investigated.

2. Experimental Details

MWCNTs were produced by arc-discharge evaporation of graphite rods (extremely pure, spectral purity, 99.9992 wt %) in the helium atmosphere (500 Torr) at current density of 175

A/cm^2 and voltage of 23 V. Material with MWCNTs was withdraw from the cathodic deposit center and had a columnar structure with the column length of up to 10 mm (Kiselev et. al., 1999). The carbon-based material containing nanotubes was only grinded and screened by using a sieve with 0.25 mm mesh without any chemical treatment.

The powdered samples of MWCNTs were fluorinated in a nickel reactor at the temperature T_F=420 °C in a flow of molecular fluorine produced by electrolyzing acidic potassium trifluoride KF·2HF containing up to 3 wt % of HF.

SWCNTs were synthesized by the electroarc method using nickel-yttrium catalyst. Amorphous carbon and metal catalyst were removed from the initial condensation products (containing 15–20 weight % of SWCNTs) by multiple alternating air oxidations at temperatures up to 550 °C and by rinsing with hydrochloric acid (Krestinin et al., 2003a). After purifying, nanotubes in the form of SWCNT powder were obtained, their main substance content being about 80–85 weight %.

Diameters of the purified nanotubes varied within a narrow range around the average value of about 1.5 nm; the nanotubes existed in the SWCNT powder in a highly aggregated state in the form of bundles, micro-crystal films, and carpets with polycrystalline structures (Krestinin et al., 2003b). SWCNTs were isolated from the main impurity by dispersing SWCNT powder in aqueous solution of surfactants. As a result, high-purity SWCNT were obtained in the form of paper (SWCNT paper) where the main substance content was over 98–99 wt %, and also there was a small dope of ultra highly-dispersed particles of graphitized soot less than 20 nm in size.

Direct fluorination was carried out in a stainless steel reactor. The SWCNT sample in an aluminum boat was placed into the reactor, which was evacuated at room temperature until the residual vapor pressure became about 10^{-1} mbar. Next, undiluted fluorine (the amount of impurities in fluorine did not exceed 0.1 volume %) was inserted into the reactor to achieve the pressure of 0.8 bar, and the reactor was heated for one hour to 222 °C (sample 1) and 190 °C (sample 2). Thereafter, the samples were kept at the given temperature for four hours more. Fluorine content was estimated by the increase in the sample weight and appeared to be 35% for sample 1 (SWCNT+F35%) and 40% for sample 2 (SWCNT+F40%).

In this work, the spectra of "white" graphite fluoride (WGF) (C_F=62.4 wt %), a highly oriented pyrolytic graphite (HOPG) crystal (Brzhezinskaya et al., 2008, 2009) and nanodiamond (Brzhezinskaya et al., 2010) were used as the reference spectra.

The C 1*s* and F 1*s* x-ray absorption spectra of the pristine and fluorinated MWCNTs, HOPG, and WGF were measured using monochromatic synchrotron radiation and the facilities of the Russian-German beamline (RGBL) at the BESSY II (Berlin) (Molodtsov et al., 2009). The samples for x-ray absorption and photoelectron measurements were prepared in air. For other details of sample preparation see (Brzhezinskaya et al., 2009).

The NEXAFS spectra were obtained by recording the TEY of the x-ray photoemission (Gudat & Kunz, 1972) in the mode of measurement of the drain current of the sample by varying the energy of incident photons. All x-ray absorption and photoelectron spectra were measured under ultrahigh vacuum (~2x10^{-10} Torr).

The energy resolutions $\triangle E$ of the monochromator in the range of the F 1*s* x-ray absorption edge ($h\nu$~680 eV) and the C 1*s* x-ray absorption edge ($h\nu$~285 eV) were equal to ~150 and 70 meV, respectively. The $h\nu$ in the range of the fine structure of the F and C x-ray absorption spectra was calibrated against the energy positions of the first narrow peak in the F 1*s* x-ray

absorption spectrum of K_2TiF_6 (683.9 eV) and the C 1*s* x-ray absorption spectrum of HOPG (285.45 eV).

In recording x-ray photoelectron spectra, *h*ν varied from 345 to 1130 eV. Energy resolution $\triangle E$ of the monochromator with the 200 μm exit slit was 145–750 meV within the above mentioned range of *h*ν. Photoelectron spectra of all the samples were measured in the normal photoemission registration mode by using the Phoibos 150 spherical analyzer from Specs whose resolution in recording the spectra remained equal to 200 meV. The analyzer was calibrated against energy based on photoelectron spectra of Au atom 4*f*7/2,5/2 electrons. The monochromator was calibrated by recording the basic photoelectron lines of C 1*s* spectra exited by radiation reflected from the diffraction grating in the first and second diffraction orders.

For more experimental details see (Brzhezinskaya et al., 2009; 2010).

3. Experimental Results and Discussion

3.1 NEXAFS spectra

Fig. 1 presents C *K*(1*s*) absorption spectra of initial SWCNTs, MWCNTs, HOPG crystal and nanodiamond measured under the same experimental conditions (Brzhezinskaya et al., 2008, 2009, 2010). All the spectra were normalized to the same level of continuous C 1*s* absorption at photon energy of 315 eV. The number and energy positions of *A*–*F* fine structure features of the initial MWCNTs, SWCNTs and HOPG C 1*s* spectra are similar. This fact confirms the crucial role a single graphene layer plays in formation of the structure of carbon 1*s* absorption spectra in HOPG, MWCNTs and SWCNTs (Brzhezinskaya et al., 2008, 2009; Krestinin et al., 2009). It also confirms that the SWCNT conduction band structure is slightly affected by nanotube curvature (Louie, 2001). In the scope of this philosophy, we associate the *A* and *B*-*C* peaks in the HOPG spectrum with dipole-allowed electron transitions from 1*s* carbon states to the unoccupied π and σ symmetry states in the conduction band that are formed from carbon $\pi 2p_z$ and $\sigma 2p_{x,y}$ states oriented perpendicular to and parallel to the carbon layer plane (graphene), respectively. Such states are mostly associated with free electron states of individual carbon atoms. The states are actually quasi-molecular as they are similar to those of benzene molecule C_6H_6 and are localized within one carbon hexagon (Brzhezinskaya et al., 2008; Comelli et al., 1988). The broad *A*' band that determines high level of continuous absorption between the *A* and *B* resonance peaks is associated with electron transitions to unoccupied π type states that are less localized in graphene layer than the state responsible for π resonance peak *A*. The broad *D*-*F* absorption bands are associated with electron transitions to the unoccupied σ states in the graphite conduction band arising due to interaction between carbon hexagons in graphene layer.

Comprehensive investigation of spectra has revealed slight differences between nanotube and HOPG spectra, as well as between SWCNT and MWCNT spectra. Those are mostly the differences in the low-energy spectral region ($h\nu$=284-295 eV). All structural features become a little broader in nanotube spectra as compared to HOPG spectrum, the broadening being different for SWCNTs and MWCNTs. This is most clearly seen for π band *A*: its full width at half maximum (FWHM) increases from 1.15 eV (for HOPG spectrum) to 1.3 eV for SWCNT spectra and up to 1.45 eV for MWCNT spectra. Moreover, for SWCNT and MWCNT spectra, extra weak structural features *a* and *a, b, c* arise in the gaps between absorption bands *A* and *B*-*C*, respectively.

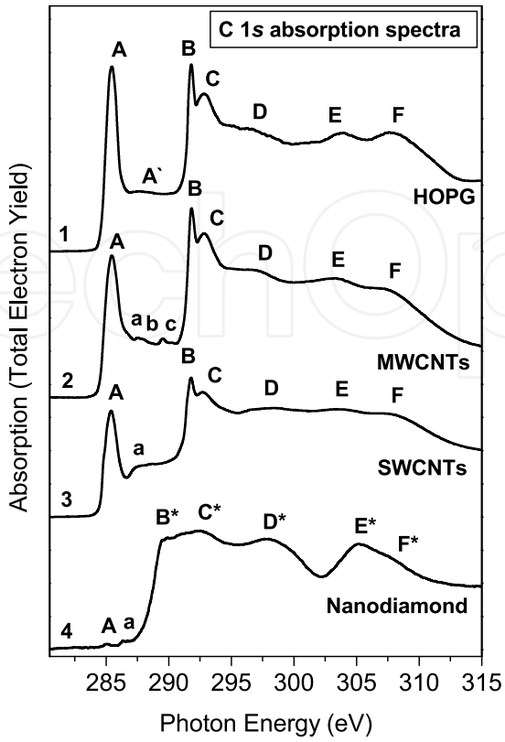

Fig. 1. C 1*s* absorption spectra of HOPG (*1*), MWCNTs (2), SWCNTs (3) and nanodiamond (4)

Naturally, the observed broadening of π band *A* in CNTs carbon spectrum as compared to HOPG spectrum can be associated with splitting of the graphite $\pi 2p_z$ conduction sub-band, which is caused by the reduction in local symmetry of nanotubes carbon atoms due to the fact that graphene layers become curved. However, for single-walled nanotubes, one should have expected greater broadening of band *A* since the SWCNT diameters (~1.5 nm) are an order of magnitude less than those of MWCNTs (~10-30 nm). In reality, as shown above, the situation is quite opposite.

In interpreting the differences in the C 1*s* absorption spectra recorded by measuring the total electron yield, it is necessary to take into account that the nanotube spectra under consideration are obtained by averaging a great number of individual SWCNTs in the bundles or in MWCNTs within the area limited by the size of the focused beam spot (0.2 x 0.1 mm^2) on the sample surface and by the probing depth (15-20 nm) (Chen, 1997). In this case, the differences in chemical states of carbon atoms in different tubes or parts of individual tubes result in energy dispersion of C 1*s* electron transitions to π symmetry electron states and, hence, can contribute significantly to broadening of π band *A*. Thus, the greater broadening of π band *A* in MWCNT spectrum may be attributed to greater variations in the carbon atom chemical states in MWCNTs as compared to SWCNTs. Greater variations in diameters and concentration of defects in the MWCNTs as compared to SWCNTs may be the reasons for this. It is also possible that just the higher degree of order of carbon atoms and their electron states in the SWCNT bundles provides high energy of interaction (about 0.5 eV per 1 nm of length) between individual SWCNTs in the bundles.

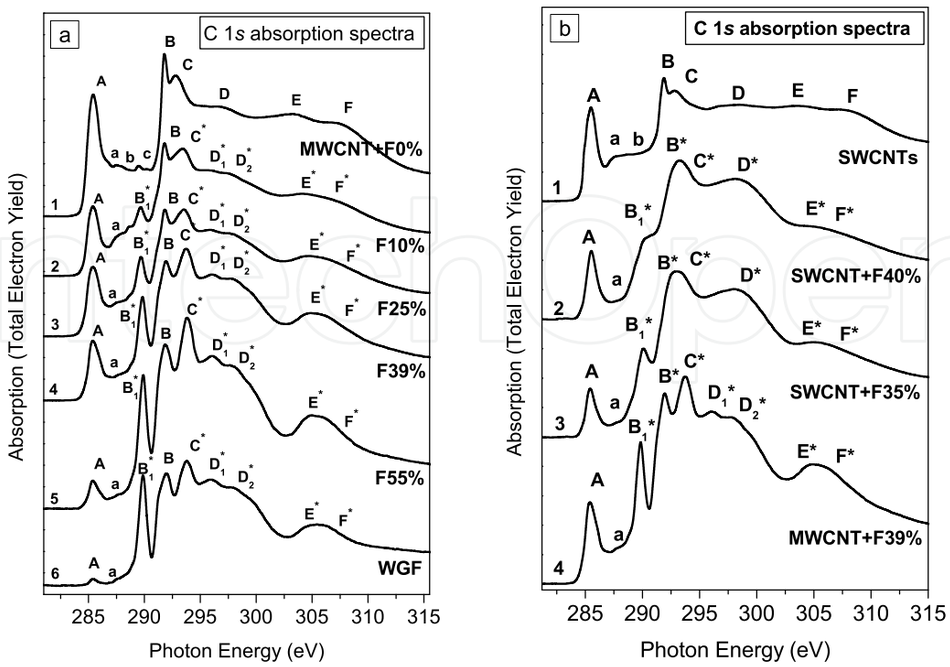

Fig. 2. (a) C 1*s* absorption spectra of (*1*) MWCNTs, (*2*–*5*) F-MWCNTs containing (*2*) 10%, (*3*) 25%, (*4*) 39%, (5) 55% and (6) WGF (62.4%); and b) C 1*s* absorption spectra of SWCNTs (1), F-SWCNTs containing 40% (2) and 35% (3) and MWCNTs+F39% (4)

In its turn, the rise of weak structures *a* and *a, b*, c between π and σ peaks in the nanotubes spectrum is typically attributed to the C 1*s* electrons transitions to free 2*p* states of carbon atoms localized on nanotube surface areas oxidized during synthesis (Banerjee et al., 2004; Kuznetsova et al., 2001). It is quite possible that the weak structures under discussion are partly associated with the 1*s*–>2*p* absorption transitions in carbon atoms at the fullerene-like edges of nanotubes.

Comparing the spectra of pristine and fluorinated CNTs (Fig. 2), we can see that their fine structures differ significantly. What is most important is that the C 1*s* NEXAFS spectra of the F-MWCNTs with the highest fluorine content (C_F=55 wt %) (MWCNTs+F55%) and WGF [Fig. 2(a), curves 5 and 6] are very similar and differ substantially from the spectra of HOPG and MWCNTs (Fig. 1, curves 1 and 2). The most significant differences involve a drastic decrease in the intensity of the resonance *A* and the band *A'* associated with the free π states and the appearance of the high-energy σ band *E**-*F**. It is evident that the observed changes are governed by the fluorination of the HOPG and MWCNTs. The resonance *A* is retained in the spectra of the fluorinated samples but has a considerably lower intensity with respect to the other spectral portion associated with the transitions of the 1*s* electrons to the free states of the conduction band. The band *B* is also retained in the spectra, whereas the other specific features in the spectra of HOPG and MWCNTs have no clear analogs in the spectra of the fluorinated samples. New specific features B_1*-*F** in the spectra of the F-MWCNTs and WGF should be unambiguously treated as a result of the transitions of the C 1*s* electrons to the free states of the new phase formed in the MWCNTs and HOPG due to their fluorination. It should be emphasized that in the given case, only one particular phase can

be formed. In the presence of several fluorocarbon phases, the C 1*s* spectra would be virtually structureless and similar in this respect to the spectrum of amorphous carbon (Rosenberg et al., 1986). Hence, the spectra of the F-MWCNTs and WGF are a superposition of the dominant C 1*s* spectrum of the fluorocarbon phase and the low-intensity spectrum of the pristine sample (MWCNTs and HOPG). In other words, despite the maximum possible fluorine content in the F-MWCNTs and WGF (55.0 and 62.4 wt %, respectively), they are incompletely fluorinated and contain regions composed of the pristine HOPG and MWCNTs. This is most probably explained by the fact that a limiting depth of fluorination exists under these conditions of the synthesis. This fluorination depth is less than the probing depth (d~15 nm) of the sample when the TEY method is employed for recording the NEXAFS spectra (Stohr, 1992; Chen, 1997). Since the sample contains MWCNTs of different sizes (L~0.5–2.0 μm and D~10–30 nm), including nanotubes with a diameter D>15 nm, the measured C 1*s* spectrum should involve the contributions of the fluorinated and pristine carbon phases.

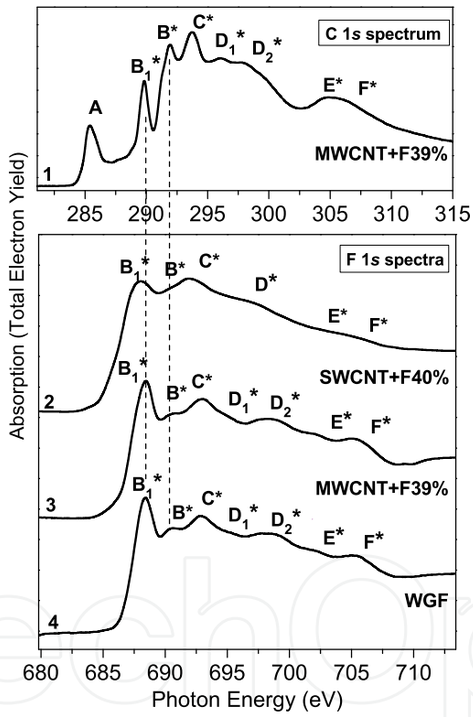

Fig. 3. Comparison of C 1*s* (1) and F 1*s* (2) NEXAFS spectra of MWCNTs+F39% and F 1*s* NEXAFS spectra of SWCNTs+F40% (3) and WGF (4). The F 1*s* absorption spectra are reduced to the energy scale of the C 1*s* absorption spectrum with the use of energy spacing ΔE(F 1*s*–C 1*s*) = 398.4 eV (measured by x-ray photoemission spectroscopy) between the F 1*s* and C 1*s* core levels.

Since the C 1*s* NEXAFS spectra of the F-MWCNTs and WGF do not contain the intense π resonance A and the π band A', we can make the inference that the C atoms are involved in the chemical bonding upon formation of the fluorocarbon phase. This implies that upon

fluorination, the F atoms are attached to the graphene layer perpendicular to it rather than replace the C atoms in the layer. In this case, the F atoms form bonds with the C atoms with the participation of the C $2p_z$ states. As a result, the C atom has a spatial coordination rather than the planar coordination.

One more indirect evidence for the change in the coordination of the C atom in HOPG and MWCNTs during fluorination can be the appearance of a single σ band E^*-F^* in the x-ray absorption spectra of the fluorinated samples ($h\nu$~303–310 eV). A similar high-energy band, together with the absence of the π resonance, is considered as a characteristic difference between the C 1*s* NEXAFS spectrum of diamond (Fig. 1, curve 4) with the sp^3 tetrahedral coordination of the C atoms and the spectrum of HOPG with the sp^2 trigonal coordination. This conclusion is in good agreement with the results obtained from the investigation into the mechanism of the formation of graphite fluoride C_xF by Raman spectroscopy (Gupta et al., 2003).

It is interesting to compare the C 1*s* x-ray absorption spectra of the F-MWCNTs with different fluorine contents (0%–55%) [Fig. 2(a)] because they correspond to different stages of the MWCNT fluorination. These spectra demonstrate a monotonic character of variations in the fine structure with an increase in the degree of MWCNT fluorination. As a result, a gradual disappearance of the π structure (the resonance *A* and the band *A*′), as well as the formation of the characteristic resonances and in the region of the σ structure in addition to a single high-energy band E^*-F^*, is observed. These changes manifest the uniform character of the interaction between the F and C atoms in all stages of the fluorination process.

In analyzing C 1*s* absorption spectra of fluorinated SWCNTs with the almost equal fluorine content of 35 and 40 wt % [Fig. 2(b), curves 2 and 3] it is necessary to notice, first of all, similarity of their general spectral shape manifesting itself in coincidence of the fine structure features number and energy positions. The only slight difference between those spectra is somewhat better resolution of band B_1^* on the spectra of the SWCNTs with lower fluorine content. Obviously, similarity of fine structures of the spectra of two fluorinated SWCNT samples reflect the similarity of their atomic and electronic structures; therefore, this confirms the reproducibility of SWCNTs fluorination results for the fluorination process described above.

Comparing the spectra of pristine and fluorinated SWCNTs, we can see that their fine structures differ significantly. Indeed, after fluorination, the only fine structure feature still remaining in the nanotube spectra is the depressed π resonance of *A*, all other features B_1^*-F^* being new. Evidently, the presence of band *A* typical of the pristine nanotube spectrum in the F-SWCNT spectra concurrently with the new absorption bands is the evidence of incomplete fluorination of single-walled nanotube bundles within the probing depth of 15-20 nm. Probably, it is caused by the fact that the SWCNT bundle fluorination depth is much shorter than the probing depth in the absorption spectra under consideration.

The above-described variations in the F-SWCNT carbon absorption spectra fine structures are quite similar but not identical to the variations observed in the structures of F-MWCNT spectrum [Fig. 2(b), curve 4] with respect to the pristine MWCNT spectrum (Fig. 1, curve 2). Indeed, Fig. 3 demonstrates clearly that, having the general form quite similar to that of spectrum of F-MWCNTs with almost the same content of fluorine (39 wt %), the F-SWCNT spectra (F35 wt % and F40 wt %) are less structured and manifest broader absorption bands. Bands B^*-C^* and D^* in F-SWCNT spectra were assumed to be the result of superposition of individual absorption bands B^* and C^*, D_1^* and D_2^* in F-MWCNT spectra.

Getting back to the differences between F-SWCNT and F-MWCNT C 1*s* spectra, we can briefly characterize them as significant broadening and blurring of prominent and well-resolved features of F-MWCNT spectrum as compared with the F-SWCNT spectra, the general spectrum shape character remaining almost unchanged. Assuming that only one fluorine-carbon phase arises in fluorination in both SWCNTs and MWCNTs, we can attribute the observed differences in their spectra to different levels of structural ordering in the phase formed. This could be due to different temperatures of nanotubes fluorination by molecular fluorine: 420 °C for multi-walled (Brzhezinskaya et al., 2008, 2009) and 190 °C and 222 °C for single-walled nanotubes. Indeed, the differences in structural ordering of fluorinated regions of single-walled nanotubes should be accompanied by differences in the strength of chemical carbon-fluorine bonding and, hence, by dispersion of charge (chemical) states of those atoms. In its turn, this should cause noticeable dispersion of energies of identical electron transitions and, hence, broadening and casual blurring of fine structure features of the carbon and fluorine absorption spectra of F-SWCNTs.

However, the nature of differences in C 1*s* absorption spectra of F-SWCNTs and F-MWCNTs is, probably, more complicated. In the case of F-MWCNTs with diameters of approximately 10 to 30 nm, the spectra under consideration are related to the major (bulk) fluorine-carbon phase due to quite large probing depth (15-20 nm) (Brzhezinskaya et al., 2009). This phase is highly ordered because of strong covalent carbon-fluorine bonding; it dominates in the F-MWCNTs over the less structured near-surface phase that coexists with the major phase within 2-3 graphene monolayers (Brzhezinskaya et al., 2009). The two phases revealed in F-MWCNTs are characterized by chemical bonding with different electron transfers between carbon and fluorine atoms, which gives rise to different carbon atomic states in those phases. Relying on these facts, we assume that, in the case of F-SWCNTs (with diameters ~ 1.5 nm), similar phases should coexist in all tubes of the bundles and, consequently, their C 1*s* absorption spectra should manifest structural features of both phases concurrently. So, blurring of fine structure features in the F-SWCNT spectra as compared to F-MWCNT spectrum may be attributed to superposition of the spectral structure features characteristic of the two fluorine-carbon phases whose carbon atoms are in different chemical states. Theoretical calculations (Ewels et al., 2006) also point to the possible presence of two fluorine super-lattices that give rise to fluorine-carbon phases with the C_4F and C_2F stechiometries on the SWCNTs lateral surface in the temperature range of 200-250 °C.

The above conclusion is confirmed by the results of comparison of the F 1*s* x-ray absorption spectra of F-MWCNTs and F-SWCNTs (Fig. 3). All the F 1*s* x-ray absorption spectra of the F-MWCNTs and WGF exhibit a similar fine structure (Brzhezinskaya et al., 2009). The main difference between the spectra is that the measured intensity of the spectra increases monotonically with respect to the background intensity with increasing fluorine content in the F-MWCNTs. This behavior of the F 1*s* x-ray absorption spectra of the F-MWCNTs with an increase in the fluorine content in the samples can be interpreted only as a result of the formation of a fluorocarbon phase, which is identical in all stages of the fluorination process. This conclusion, of course, should correlate with the probing depth (~15 nm) of the nanotube samples during the recording of the x-ray absorption spectra in this work. The F 1*s* x-ray absorption spectra are also characterized by rich and clearly pronounced fine structure. This circumstance indicates a well-defined atomic structural order in the

fluorinated samples. In other words, the fluorine atoms, such as the carbon atoms, have an identical coordination, which reflects chemical bonding of the C and F atoms.

The above-made conclusion on the covalent character of fluorine-carbon bonds in F-MWCNTs and retention of laminar character of the carbon atomic structure up to maximal fluorine concentrations ensuring the binary (CF) stoichiometry of fluorination products agrees well with wellknown results of graphite fluorination. It was found out for graphite that when it is maximally fluorinated, fluorinecarbon phase poly(carbon monofluoride) $(CF)_n$ predominates (Gupta et al., 2003; Sato et al., 2003) which is characterized by the retention of laminar graphitelike structure, although the layers are no longer planar but become corrugated because fluorine atoms are attached to them. What is important is that this graphite fluoride is characterized by covalent binding with sp^3 hybridization of carbon-atom valent states. This fact is confirmed also by the similarity of absorption spectra of F-MWCNTs and WGF reference samples. All this confirms the above conclusion that MWCNTs retain their basic structure at high fluorination levels, such as 55 wt %, where almost every carbon atom throughout all CNT layers is in the sp^3 configuration.

F 1*s* absorption spectra of F-SWCNTs with almost the same fluorine content of 35 and 40 wt % are in general similar: numbers of their spectral features are identical, their energies are close to each other (Brzhezinskaya et al., 2010). The only slight difference between them is somewhat better fine structure resolution of the spectra of tubes with less fluorine content; this is clearly seen when comparing the B_1* bands.

It is very important that both F 1*s* and C 1*s* absorption spectra of F-SWCNTs are, in general, very similar to respective F-MWCNT spectra (Fig. 3, curve 4). The main difference is that the fluorine spectra for F-MWCNTs are better structured (as the carbon spectra are). This fact clearly confirms our conclusion made above that the major covalent fluorine/carbon phases arising in fluorination of single- and multi-walled nanotubes are similar to each other. Hence, we can assume that SWCNT fluorination occurs mainly by bonding fluorine atoms to carbon atoms on nanotube sidewalls (similar to MWCNT fluorination); this is accompanied by generation of σ(C-F) bonds by covalent mixing of valence F 2*p* and C $2p_z\pi$ electronic states without any destruction of the tubular structure of carbon layers (Brzhezinskaya et al., 2008, 2009). Such fluorine bonding transforms carbon triangular arrangement of initial nanotubes into almost tetrahedron one of fluorinated nanotubes, which becomes possible only if sp^2 hybridization of carbon atom valence states in pristine nanotubes transforms into sp^3 hybridization of F-SWCNTs. Such transformation of atomic structure should cause corrugation of nanotube sidewalls.

It is interesting to analyze the fluorinated sample unoccupied electronic state spectrum by using C 1*s* and F 1*s* X-ray absorption spectra that reflect energy distribution of free electron states formed from the 2*p* states of the carbon and fluorine atoms, respectively, because of the dipole nature of absorption transitions. For this purpose, the carbon and fluorine atom spectra for F-MWCNTs with the 35 wt % fluorine content (curves 1 and 3) are given in Fig. 3 on the photon energy scales that are brought into coincidence by using the ΔE (F 1*s* – C 1*s*) =398.4 eV energy shift between the fluorine and carbon 1*s* states in the system. In this work, energy positions of the core levels were measured the by X-ray photoemission technique at the exciting photon energy of 1030 eV.

Comparing the spectra, we can clearly see that both spectra manifest fine structures similar in the number and energy positions of their key features B_1*-*F** (the *A* band in the carbon spectrum is associated with non-fluorinated tubes). Vertical dashed lines in Fig. 3 indicate

that energy positions of bands B_1 and B^*-C^* in the carbon and fluorine absorption spectra of F-SWCNTs and F-MWCNTs are close to each other. Such correlation in the F-CNT carbon and fluorine spectra means that carbon and fluorine 1*s* electron transitions to the unoccupied electronic states formed from C 2*p* and F 2*p* electronic states are responsible for the key features of the spectra compared. It indicates the hybrid (covalent) F 2*p* + C 2*p* nature of the free electronic states in the systems discussed, which complies with the conclusion about sp^3 hybridization of the carbon atom valence states, which was made as a result of independent analyses of carbon and fluorine spectra.

3.2 XPS spectra

X-ray photoelectron spectra of SWCNTs and MWCNTs were measured by using exciting photons with energies from 385 to 1030 eV. All the measurements were carried out under the same experimental conditions. For both SWCNTs and MWCNTs, the *A* line in the C 1*s* spectra is a narrow peak at *BE*=284.8 eV which is asymmetrically shaped at the higher binding energy side and whose full-width at half maximum (FWHM) is 0.7 eV.

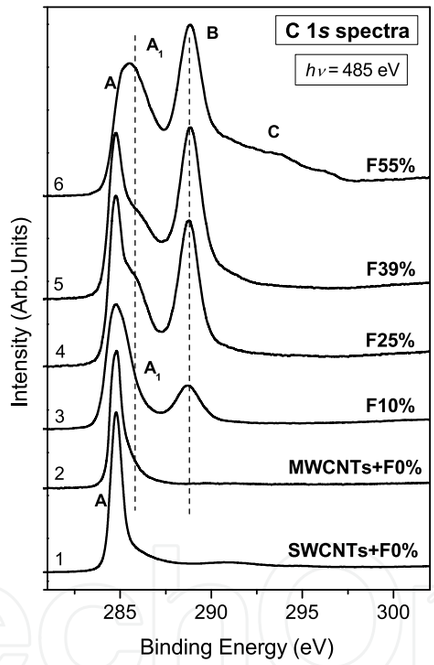

Fig. 4. C 1*s* x-ray photoelectron spectra of (1) SWCNTs, (2) MWCNTs and F-MWCNTs with fluorine concentrations: 10% (3), 25% (4), 39% (5), 55% (6).

Fig. 4 demonstrates that C 1s photoelectron spectrum structure changes radically as pristine MWCNTs are transformed into F-MWCNTs. Shoulder A_1 shows up near the main line *A* at *BE*=285.7 eV, and the second line *B* arises at *BE*=288.8 eV. As the fluorine concentration in F-MWCNTs is growing, the intensities of the spectrum new features increase, while their energy positions do not change. When the concentration reaches C_F=39 wt %, intensity *B* becomes almost equal to the main C 1*s* line intensity *A*. Spectrum measured at the maximum fluorine concentration (C_F=55 wt %) differs significantly from the other spectra: band *A*

almost fully disappears against the background of the intense band into which shoulder *A* is transformed, whereas band *B* becomes the most intense structure feature having an intense, extended and poorly structured tail *C* on the high-energy side.

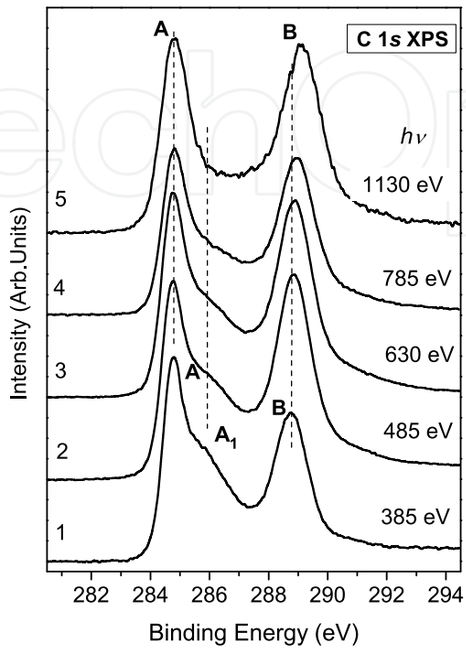

Fig. 5. C 1*s* x-ray photoelectron spectra of MWCNTs+F39% measured at photon energies of 385 eV (1), 485 eV (2), 630 eV (3), 785 eV (4) and 1130 eV (5).

As shown in our work (Brzhezinskaya et al., 2009), appearance of new features in the F-MWCNT C 1*s* spectra structure as compared with those of MWCNTs can be attributed to CNT fluorination; therefore, it can be regarded as a result of carbon-fluorine chemical bonding. This interaction results in formation of fluorine-carbon phases and is accompanied by charge transfer from carbon atoms to fluorine atoms due to the fact that fluorine electronegativity is higher. Charge states (oxidation rates) of carbon atoms in at least two of the fluorine-carbon phases are different and can be characterized by chemical shifts of their C 1*s* photoelectron lines (peaks A_1 and *B*) from the energy position of this line in pristine MWCNT spectrum (peak *A*). Energy positions of bands A_1 and *B* relative to peak *A* are significantly different (0.9 eV and 4.0 eV, respectively). This large difference (>3 eV) indicates considerable differences in the natures of C-F atom interactions in the analyzed fluorine-carbon phases that are formed in F-MWCNTs.

Relative intensities of bands *A* and *B* do not change much with *hν* increasing up to 1030 eV, while the A_1 band intensity decreases, and the corresponding shoulder gets barely visible against band *A* background. It is reasonable to connect those observations with the probing depth increase from ~0.6 nm (1-2 graphene layers) to 2 nm (5-6 layers). The weak relationship between the peaks *A* and *B* relative intensities indicates that the ratio of the initial and fluorinated MWCNTs phases for the samples with C_F=10–39 wt % changes only slightly with depth within several graphene layers. This statement is consistent with the

conclusion that the fluorination process in MWCNTs under investigation remains uniform within the depth limits of ~15 nm (Brzhezinskaya et al., 2008).
A significant decrease in the band A_1 intensity with the probing depth increase from 0.6 to 2 nm shows unambiguously that phase 2 is of the near-surface character and is formed by fluorination of only a few outer graphene layers. This conclusion is consistent with the specific shape of C 1*s* photoelectron spectrum obtained for MWCNTs+F55%.

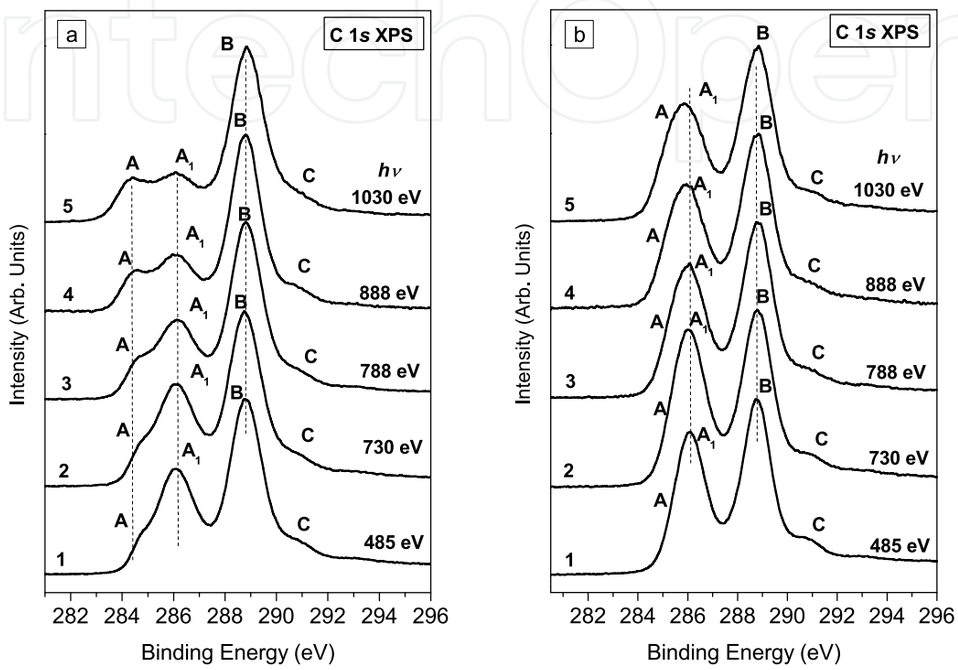

Fig. 6. C 1*s* x-ray photoelectron spectra of (a) SWCNTs+F35% and (b) SWCNTs+F40% measured at photon energies of 385 eV (1), 730 eV (2), 788 eV (3), 888 eV (4), 1030 eV (5).

The energy gap between bands *A* and *B* grows by ~0.5 eV as photon energy changes from *h*ν=385 eV to *h*ν=1130 eV. It means that chemical shift of the C 1*s* level grows from 4.0 to 4.5 eV with increasing probing depth for spatial fluorocarbon phase. Such an increase in the chemical shift is observed for *h*ν>700 eV only. It may be a result of a small change in the chemical state of phase 1 carbon atoms located deeper in the samples. In this case, the chemical shift of 4.5 eV for C 1*s* level is practically equal to the 4.45 eV chemical shift in the C 1*s* absorption spectra (Brzhezinskaya et al., 2008).
The feature A_1 behavior is similar in all F-MWCNTs spectra; Fig. 5 represents MWCNT+F39% to illustrate this fact. The band A_1 intensity gradually decreases with increasing probing depth (d=0.4–2 nm and *h*ν=345–1130 eV). It is reasonable to connect the gradual band A_1 weakening with formation of fluorocarbon phase in the very near-surface layer of the tubes. This layer is one to two graphene monolayers thick as this is just the depth (0.4–0.8 nm), where from C 1*s* photoelectrons generated by absorption of photon with *h*ν=345–630 eV and having kinetic energies of E_k=60–345 eV can be emitted without energy losses (Huefner, 2003; Brown et al., 1978; Martin et al., 1985).

The spectra of F-SWCNTs (Fig. 6) were measured at photon energies from 385 to 1030 eV. According to the universal curve of electron mean free path versus kinetic energy (Brzhezinskaya et al., 2009), the escape depth of C 1*s* photoelectrons excited by photons with energies of 385 to 1030 eV varies from about 0.5 to 1.5 nm; thus, the probing depth lays actually within the subsurface layer about one nanotube diameter wide. As compared with F-MWCNTs (Fig. 4), for F-SWCNTs, C 1*s* photoelectron spectrum structure changes even more radically as initial SWCNTs are being transformed into F-SWCNTs. In the C 1*s* photoelectron spectrum of SWCNTs+F35%, there are 4 peaks, *A* (*BE*=284.6 eV), A_1 (*BE*=286.1 eV), *B* (*BE*=288.8 eV) and *C* (*BE*=290.9 eV). Notice that at small photon energies (<888 eV) band *A* manifests itself as a shoulder next to peak A_1 on the lower binding energy side. In the C 1*s* spectra of SWCNTs+F40% there are only three explicit features: bands A_1 (*BE*=286.1 eV), *B* (*BE*=288.8 eV), and shoulder *C* (*BE*=290.9 eV). The presence of band *A* is indicated by only the large width and slight low energy asymmetry of band A_1. Coincidence of bands A_1 positions and bands *B* positions in the F-SWCNTs and F-MWCNTs indicates their connection with two fluorine-carbon phases that are similar for the single- and multi-walled nanotubes. This fact indicates their relation to two different fluorine-carbon phases that are respectively similar in single- and multi-walled nanotubes. As shown above, a single fluorine-carbon phase uniformly distributed within the sample probing depth is formed in fluorination of both MWCNTs and SWCNTs. Peak *B* in C 1*s* photoelectron spectra of F-MWCNTs is attributed to this phase. Then the same peak *B* should correspond to this phase in the F-SWCNT C 1*s* photoelectron spectra.

Energy positions of bands A_1, *B* and *C* relative to peak *A* are significantly different (1.3 eV, 4.0 eV and 6.1 eV, respectively) for SWCNTs+F35%. For SWCNTs+F40%, energy shifts of peaks A_1, *B* and *C* are the same when measured relative to peak *A* energy position for SWCNTs+F35%. Note that peak *A* cannot be clearly identified in the SWCNTs+F40% spectra [Fig. 6(b)]. This large difference (~3 and 6 eV) indicates considerable differences in the natures of C-F atom interactions in the analyzed fluorine-carbon phases formed in F-SWCNTs.

It is interesting that in the C 1*s* spectra of SWCNTs+F35% [Fig. 6(a)] measuring with photon energy increasing from 485 to 1030 eV and, hence, with probing depth increasing from ~0.5 nm to ~1.5 nm, band A_1 relative intensity becomes more than twice lower than that of band *B*. Probably, this indicates a significant decrease in the fluorination level of inner nanotubes located inside the bundle, namely, all the nanotubes that do not participate in forming the bundle surface layer. This conclusion correlates well with the earlier revealed increase in the SWCNT fluorination level accompanied by improvement of their dispersion, i.e., by the decrease in transverse size of the bundles formed by the nanotubes (Krestinin et al., 2009). However, the decrease in SWCNTs+F40% band A_1 intensity is not so dramatic [Fig. 6(b)]. Generally, shapes of SWCNTs+F40% [Fig. 6(b)] and MWCNTs+F55% (Fig. 4, curve 5) C 1*s* spectra are similar, except for the band *C* shape.

Thus, the first fluorine-carbon phase (phase 1, peak *B*) is apparently formed by fluorine atoms covalent bonding with the graphene layer. Contrary to phase 2 (peak A_1), this phase is uniformly distributed within the sample probing depth (0.5-1.5 nm for XPS). Moreover, this fluorine-carbon phase contributes most to C 1*s* absorption spectra of fluorinated nanotubes at larger probing depths (Brzhezinskaya et al., 2010). In addition, just phase 1 is associated with formation of the C_2F super-lattice on the surfaces of both F-SWCNTs and F-MWCNTs.

This is confirmed by most theoretical calculations (Bettinger et al., 2001; Kudin et al., 2001; Seifert et al., 2000).
Chemical shift in the second phase (phase 2, peak A_1) of the C 1*s* electron binding energy (1.2 eV) is significantly smaller than that in the first phase (4.0 eV). Hence, unlike phase 1, phase 2 formation is accompanied by significantly lower carbon-fluorine electron density transfer resulting in a weaker chemical bond. Phase 2 is most probably associated with formation of C_4F superlattice on the surfaces of both F-SWCNTs and F-MWCNTs. This idea is consistent with the calculation results (Ewels et al., 2006) showing that the most stable phase is (1,2) (C_2F) phase followed by the (1,4) (C_4F) phase. When the probing depth increases from ~0.5 nm to ~1.5 nm, the band A_1 intensity decreases relatively to the band *B* intensity. For F-SWCNTs, such a transformation of band A_1 is likely to confirm the above conclusion about incomplete SWCNT fluorination inside the bundles. Therefore, phase 2 is developed only on SWCNTs located in the bundle near-surface layers, at least SWCNTs located on the bundle outer periphery having the greatest chance to become completely fluorinated. It is known that individual SWCNTs are arranged in the bundles almost coaxially and practically without tangles, the number of tubes per bundle being about 300. The F-SWCNT defluorination experimental results discussed below also point to a weaker carbon-fluorine bond.

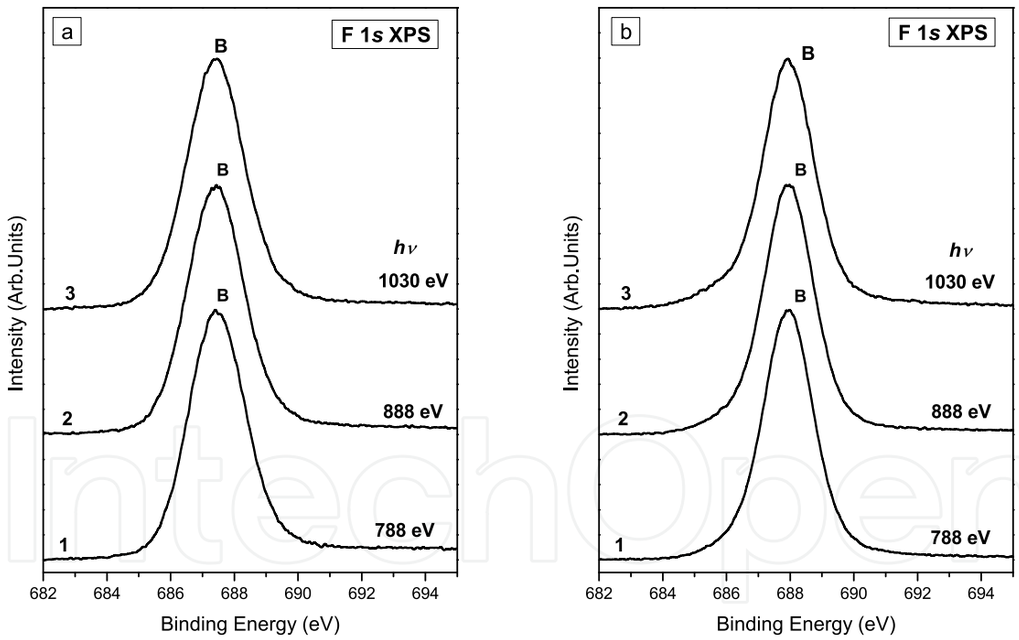

Fig. 7. F 1*s* x-ray photoelectron spectra of (a) SWCNTs+F40% and (b) MWCNTs+F39% measured at photon energies of 788 eV (1), 888 eV (2), 1030 eV (3).

In addition to new peaks A_1 and *B* in the F-SWCNT C 1*s* photoelectron spectra there is one more feature *C* whose intensity is significantly lower than that of peaks *A*-*B*. Feature *C* is approximately 6 eV apart peak *A* itself in the case of SWCNTs+F35% or from peak *A* assumed position in the case of SWCNTs+F40%. In this case, chemical shift of feature *C*

carbon atom 1*s* electron binding energy (~6 eV) is much larger than the shift corresponding to phase 1 (4.0 eV). Hence, this peak is obviously associated with F-SWCNT carbon atoms with higher oxidation levels as compared with carbon atoms of phase 1. Relative intensity of peak *C* is independent of the excited photon energy (Fig. 6). It is possible that, contrary to MWCNTs, an extra fluorine-carbon phase 3 is formed as a result of SWCNT fluorination. As compared with phase 1, formation of phase 3 is accompanied by even higher carbon-fluorine electron density transfer resulting in formation of a stronger chemical bond. Phase 3 is probably formed due to covalent bonding of fluorine atoms to carbon atoms on the SWCNT open edges. Theoretical calculations performed for nanographite and STM measurements (Saito et al., 1999; Maruyama et al., 1994; Kobayashi et al., 2005) also point to such possibility. Notice that destruction of nanotube fullerene-like edges is a particular feature of just the SWCNT purification process (Krestinin et al., 2003). If this is true, fluorine atoms should be able to get attached to SWCNT graphene mesh not only by sharing carbon atom $2\pi p_z$ orbitals but also by using dangling $2\sigma p_{x,y}$ bonds at the SWCNT graphene mesh edges at the points where fullerene-like structures were previously attached. This would result in formation of even stronger carbon-fluorine chemical bond of the CF type due to covalent mixing of the F 2*p* and C $2\sigma p_{x,y}$ electron states.

(Saito et al., 1999) showed, the fluorine atoms get first attached to the edge carbon atoms and only later they begin bonding to carbon atoms located along the nanotube perimeter. It was shown that doped F is more stable at the edge than in the interior region. The dopant´s electron is strongly localized around the F site, and even two F atoms can interact with a single carbon atom, i.e., CF_x (x>1) clusters are formed. There are two ways for fluorine atoms to get attached to the edges of nanotubes: by forming either Klein`s bearded zigzag edge (Klein, 1994) (two fluorine atoms are attached to a single carbon atom at the edge) or Fujita`s normal zigzag edge (Fujita et al., 1996) (one fluorine atom is attached to one carbon atom). This conclusion is confirmed by the peak *C* behavior in the process of SWCNTs+F40% thermal defluorination (see below), which shows that, contrary to peaks *B* and A_1, peak *C* can not be totally reduced. Seifert et al., 2000 calculated that equimolar $(CF)_n$ nanotubes are stable. However, the authors believe that formation of stable $(CF)_n$ nanotubes may be hindered by the height of the energy barrier preventing fluorine atoms penetration into CNTs. But in our case, when the most part of fullerene-like nanotube edges are already destructed, it is easier for fluorine to penetrate into SWCNTs.

This difference in carbon atom chemical states in the fluorine-carbon phases compared should manifest itself in different spatial structures, particularly, in the increase of interatomic spacing when moving from phase 1 to phase 2 and then to phase 3.

F 1*s* spectra with $h\nu$=788–1088 eV were also measured for F-SWCNTs and F-MWCNTs (Fig. 7). Here the photoelectron kinetic energies were about E_k~100-400 eV, which corresponds to the probing depth of about d~0.5÷1.0 nm. F 1*s* spectra of SWCNTs+F35% and SWCNTs+F40% are the same. F 1*s* photoelectron spectra of F-MWCNTs keep their energy positions and, contrary to the C 1*s* spectra, do not exhibit any significant changes in their shapes up to C_F=39 wt %. F 1*s* photoelectron spectra of F-CNTs [(Fig. 7(a)] consist of the main peak *B* only. The binding energy corresponding to the F 1*s* peak of F-SWCNTs is *BE*=687.4 eV; it is shifted by 0.5 eV towards smaller *BE* as compared with MWCNTs+F39% (*BE*=687.9 eV) [Fig. 7(b)] (Brzhezinskaya et al., 2009). At the same time, its FWHM is 2.1 eV, which is 0.2 eV larger than that of F 1*s* peak of F-MWCNTs (1.9 eV).

F 1*s* spectra are less informative as compared to C 1*s* spectra. The effective charge of fluorine atom in F-SWCNTs, as in the most of other compounds, is negative and varies in a limited range of 0 to -1 when the atom´s chemical state changes. A small change in the valence electron density in a fluorine atom is accompanied, due to its participation in chemical bonding with carbon atoms, by a weak change in screening of F 1*s* core level electrons by valence electrons, which manifests itself in small values of chemical shifts of F 1*s* electron bonding energies.

Thus, the fluorine spectrum is a superposition of contributions from all the F 1*s* electrons involved in chemical bonds with carbon atoms. In the case of F-SWCNTs, there is one extra fluorine-carbon phase with much stronger fluorine-carbon bond (as compared with the other two phases observed also in F-MWCNTs) and, hence, with greater carbon-fluorine electron charge transfer. C 1*s* photoelectron spectra showed that the phase 3 contribution is smaller than that from phases 1 and 2, and, hence, the shift of the F-SWCNTs F 1*s* peak as a whole towards the lower binding energies is also insignificant (0.5 eV).

3.3 Results of defluorination experiments

Investigation of CNT defluorination process makes it possible to estimate the type and power of carbon-fluorine bonding and to find out whether the graphene mesh is distorted. Thermal annealing is one of the possible methods of F-CNT defluorination. Our data obtained for F-MWCNT annealing (Brzhezinskaya et al., 2009) showed that annealing started at temperatures almost equal to the fluorination temperature (T_F). As was shown above the results of fluorination process is more complicated for F-SWCNTs (Brzhezinskaya et al., 2010). Therefore, the results of defluorination experiments are presented here for F-SWCNTs only (for F-MWCNTs see Brzhezinskaya et al., 2009). The thermal annealing process was controlled by both NEXAFS and XPS.

The first changes in the C 1*s* absorption spectrum structure of SWCNTs+F40% were observed only after the fifth annealing carried out temperature close to T_{DF} and T_F of F-MWCNTs (T_A=350 °C) [Fig. 8(a) and 8(b), curves 2]. The changes manifested themselves in small reduction of bands B_1* and D* relative intensities and growth of bands A and B intensities [Fig. 8(a), curve 3]. Bands B_1* and D * in the C 1*s* absorption spectrum correspond to the transitions of C 1*s* electrons to the free hybridized states formed from C 2*p* and F 2*p* states. Bands A and B correspond to the spectra of the pristine regions of hexagonal graphene mesh without any fluorine atoms attached. At the same time, no changes are observed in F 1*s* spectrum features [Fig. 8(b), curve 3]. Obviously, such changes in C 1*s* and F 1*s* absorption spectra of F-SWCNTs [Figs. 8(a) and 8(b), curves 4] demonstrate the onset of defluorination process, i.e., partial breakage of C-F bonds, which, apparently, occurs mainly in the outer SWCNTs in SWCNT bundles. After the eighth annealing performed at T_{DF}=420 °C, defluorination becomes even more evident, namely, the F 1*s* spectrum begins changing as intensely as the C 1*s* spectrum does [Figs. 8(a) and 8(b), curves 5]. Therefore, F-SWCNT and F-MWCNT defluorination temperatures are equal to each other and to the F-MWCNT fluorination temperature (T_{DF}=T_F=420 °C). This fact seems to be quite natural. It is generally recognized that the rolling of the graphene sheet induces strain, but for large-diameter CNTs the strain energy per carbon atom E_s is small. It was shown that E_s~D^{-2}, where D is the tube diameter (Mitmire & White, 1997; Hernandez et al., 1999). That is why the chemistry of wide CNTs should be similar to that of graphite, whereas the narrower tubes are expected to be more reactive due to larger strain of the carbon framework (Bettinger, 2001). Accordingly,

fluorination temperature of SWCNTs with 1.4-1.6 nm in diameter (T_F~200 °C) is much lower than fluorination temperature of MWCNTs with 10-30 nm in diameter. We have demonstrated that the absorption and photoelectron spectra of F-SWCNTs and F-MWCNTs and, hence, SWCNT and MWCNT fluorination results are similar, which manifests itself in covalent attachment of fluorine atoms to carbon atom $\pi 2p_z$ orbitals. Thus, at least two of the fluorine-carbon phases formed as a result of fluorination are identical in F-SWCNTs and F-MWCNTs, and, hence, the carbon-fluorine chemical bonds within each phase are equally strong. Consequently, the same amount of energy is needed to break those bonds in either of the tube types. It is due to this that the defluorination temperatures of F-SWCNTs and F-MWCNTs are equal.

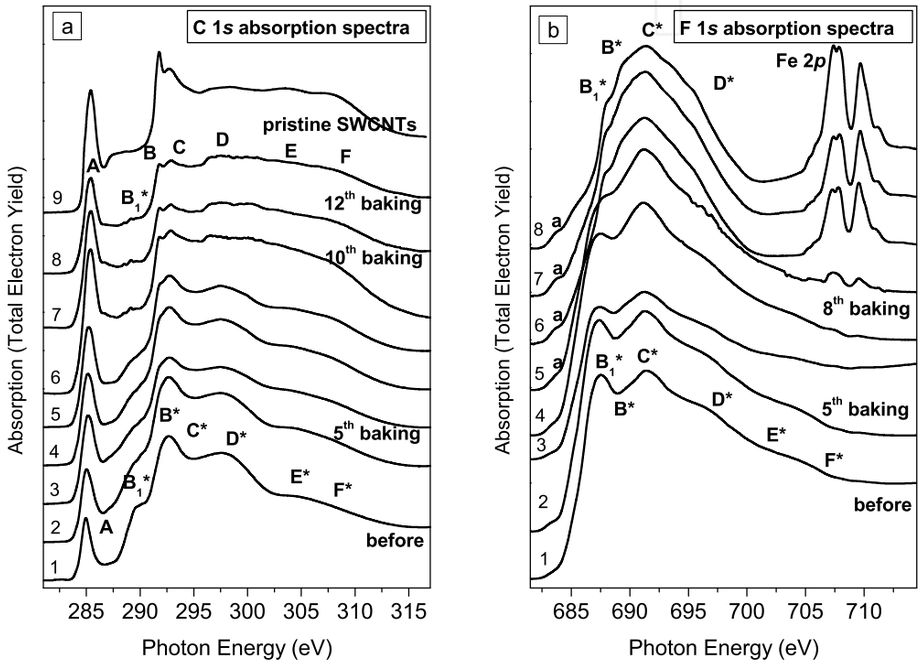

Fig. 8. (a) C 1*s* and (b) F 1*s* absorption spectra of SWCNTs+F40% before and during annealing

Notice that even the last 12th annealing did not ensure complete defluorination of F-SWCNTs. It appears from the fact that band B_1*, though dramatically reduced, is still retained on the C 1*s* absorption spectrum of F-SWCNTs. This fact indirectly confirms the presence of phase 3 with stronger fluorine carbon bonds than in phases 1 and 2.

Contrary to the C 1*s* spectrum, the F 1*s* absorption spectrum [Fig. 8(b)] changes stepwise. The intensities of bands B_1*-*F** drop instantly, the absorption spectrum as a whole becomes less structured. From the above, it is reasonable to believe that at $T_{DF}=T_F$ (MWCNTs) intense breakage of earlier formed C-F bonds takes place. Therefore, we can assume that the hexagonal carbon mesh destruction is insignificant, though more significant than in this case of F-MWCNTs. This is demonstrated by restoration of C 1*s* spectrum features typical of the initial MWCNTs and HOPG (π resonance *A*, σ resonance *B*, bands *D*-*F*). Such restoration of the *A*-*F* bands takes place concurrently with the reduction of bands associated with the transitions of C 1*s* electrons to the hybridized C-F states (bands B_1*-*F**). Such a behavior of

the main spectrum features does not contradict the interpretation of new absorption bands arising in C 1*s* spectra of F-SWCNTs after fluorination as those reflecting the C 1*s* electrons transition to the hybridized C-F states of the new C-F phase.

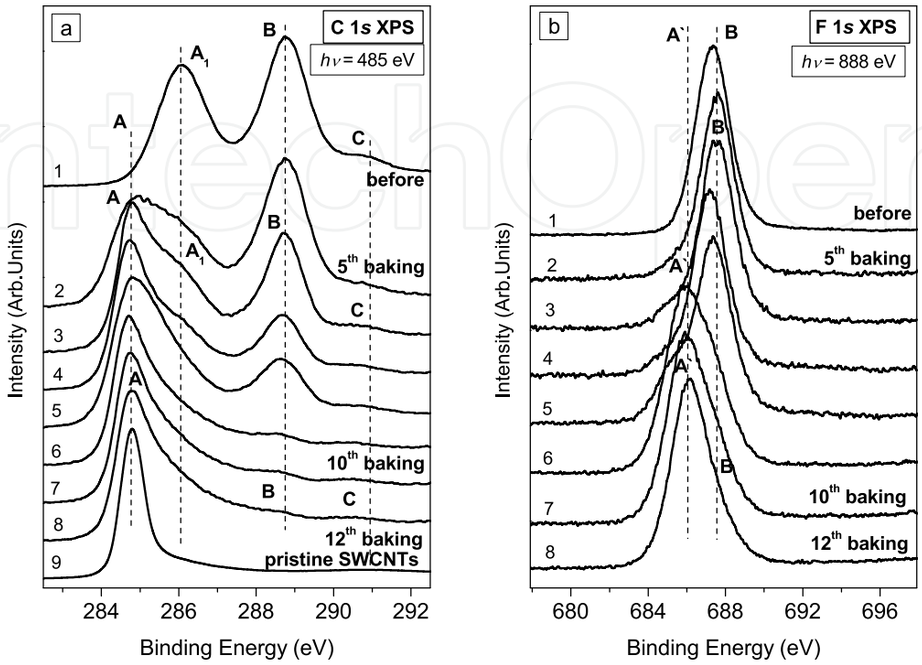

Fig. 9. (a) C 1*s* and (b) F 1*s* x-ray photoelectron spectra of SWCNTs+F40% before and during annealing

Actually, defluorination of F-SWCNTs is accompanied by modification of the *E**-*F** bands typical of sp^3 hybridized electron states of carbon atoms into the *E* and *F* bands typical of HOPG with sp^2 hybridization of electron states of carbon atoms. After the further annealing of the sample (T_{DF}=440 °C), the C 1*s* spectrum features reduced after fluorination were restored almost fully [Fig. 8(a), curves 6-8], whereas the F 1*s* spectrum varies only slightly [Fig. 8(b), curves 6-8]. The most important modification of the latter is the emergence of new features at hv=704–713 eV after the 8th annealing. Those new features became well pronounced in Fe 2*p* absorption spectrum [Fig. 8(b), curves 6-8] after the 9th annealing. It should be noticed that, upon the 12th annealing, F 1*s* spectrum does not look like HOPG or CNT spectrum any more. As in the case of the F-MWCNT absorption spectra, we can assume that F 1*s* absorption spectra of F-SWCNTs become similar to the 3*d* transition-metal fluorides spectra. It is notable that in the spectrum there is an extra low-energy structure, namely, feature *a* (hv= 683.6 eV) that is caused by transitions of the F 1*s* electrons to low-lying empty electronic states with the e_g and t_{2g} type symmetry of the transition-metal 3*d* – fluorine 2*p* hybridized character (Vinogradov et al., 2005). In addition, a broad band (~15 eV) at the photon energies of 685-700 eV becomes more and more pronounced in the spectrum structure at the last stages of annealing (after the 9th annealing); this band is caused by core-electron transitions to the unoccupied $4sa_{1g}$ and $4pt_{1u}$ electronic states of the transition-metal atom hybridized with the 2*p* states of the ligand atoms. Notice that the Fe 2*p* spectrum consists of two bands whose intensities grow with heating. Thus, that it is not only

the stainless steel sample holder responsible for the signal detected but that fluorine-iron interaction has happened as a result of F-SWCNT defluorination. The presence of two spectral bands under consideration is, most probably, the result of superposition of the iron spectra from the stainless steel and iron fluorides. The substrate signal is detected not only in the absorption spectra (probing depth of 15 nm) but also in overall photoelectron spectra measured at 1030 eV (probing depth of 1.5 nm). This may be the evidence of micro-cracks formation in the sample (the micro-crack number increasing with the annealing time), since no visible cracks were detected in the sample even after the end of heating.

To our point of view, the scanning transmission microscopy (STM) results (Kelly et al., 1999) support this idea. STM images present the fluorinated zones as well-defined closed rings along the nanotube perimeters. At the same time, complete fluorination of C_2F results in radial distortions of CNTs (van Lier et al., 2005). Therefore, we can assume that thermal defluorination of SWCNTs may result in both destruction of bundles and slight distortion of nanotubes themselves. The first of the processes is more probable and preferable as our F-SWCNTs absorption and photoemission spectra show no evidence of any significant amount of amorphous phase in the samples after annealing.

The F 1*s* spectrum shape after the 12th annealing possibly points to formation of iron fluoride FeF_x. These findings (fluorination of metal substrate) testify that separate fluorine atoms are mainly detached during the thermal defluorination of F-SWCNTs, as we found for F-MWCNTs also (Brzhezinskaya et al., 2009). Moreover, formation of FeF_x indirectly proves that in defluorination C-F bonds get broken and fluorine is ejected from the sample not in the form of CF_x clusters but in single atoms as in the case of F-MWCNTs.

At the same time, there is significant difference between F-SWCNT and F-MWCNT defluorination results. For F-MWCNTs, the identity of C 1*s* absorption spectra of defluorinated F-MWCNTs and pristine MWCNTs points to the absence of any remarkable amount of amorphous component in the sample after annealing. As for F-SWCNTs, thermal annealing did not result in complete restoration of resonance *B* associated with C 1*s* electron transitions to the unoccupied σ symmetry states in the conduction band, which arise from $\sigma 2p_{x,y}$ carbon atomic states. This may be the evidence of partial distortion of SWCNT graphene mesh in fluorinated zones provided we assume them to be located around the tube circumference (van Lier et al., 2005). On the other hand, defluorination can lead to destruction of the outer (fully fluorinated) tubes of the bundles and to the increase in the C 1*s* absorption spectrum signal from non-fluorinated tubes from the bundles inner parts. The π resonance is restored almost completely. Therefore, we can conclude that SWCNTs are destructed by defluorination only scarcely, the destruction manifesting itself as a small number of point defects in the graphene mesh. At the same time, defluorination still destructed a negligible number of tubes, which resulted in emergence of a small amount of amorphous component in the sample; the evidence of this fact was some blurring in the high-energy region of the C 1*s* absorption spectra ($h\nu$=295-315 eV) after the 12th annealing [Fig. 8(a), curve 8]. Such blurring may also be the result of incomplete fluorination of SWCNTs in the bundles or of the existence of two different ways of graphene fluorination: the first one is that fluorine atoms are attached to positions (1,2) of the carbon hexagons, the second one is that they get attached to positions (1,4) (Ewels et al., 2006; Khabashesku et al., 2002). These two types of fluorine atoms attachment to carbon correspond to the two fluorine-carbon phases described above (C_2F and C_4F, respectively). As both structures are assumed to be formed on a nanotube wall concurrently (Khabashesku et al., 2002), transition

zones with low fluorination degree would appear along the boundaries of the zones with different types of fluorine attachment. On the other hand, defects can emerge in the transition regions in the process of defluorination (Khabashesku et al., 2002).

The photoelectron spectra (Fig. 9) analysis supports our conclusions about the defluorination processes in F-SWCNTs. The first changes in the C 1*s* photoelectron spectrum structure were observed only after the firth annealing carried out at the temperature close to T_{DF} and T_F of F-MWCNTs (T_{DF}=350 °C) [Fig. 9(a), curves 2]. The changes manifested themselves in big reduction of peak's *B* and small reduction of peaks' *B* and *C* relative intensities and growth of peak's *A* intensity [Fig. 9(a), curve 3]. Peak *A* corresponds to the spectra of the pristine regions of hexagonal graphene mesh. Fig. 9(a) shows that the band A_1 intensity decreases drastically, and peak *A* increases with respect to band *B* already at the first stages of annealing. Hence, such a behavior of peak A_1 during annealing is unambiguously consistent with its interpretation as a signal from carbon atoms forming a fluorine-carbon phase with fluorine-carbon chemical bond weaker than the bond in phase 1.

At the same time, contrary to F 1*s* absorption spectrum, F 1*s* photoelectron spectrum begins to change after the 5th annealing [Fig. 9(b), curve 3]. Shoulder *A`* arises on the low-energy side of peak *B*. These findings become even more evident after the annealing at T_{DF}=400°C. Obviously, such changes in C 1*s* and F 1*s* photoelectron spectra of F-SWCNTs [Figs. 9(a) and 9(b), curves 4] demonstrate the onset of defluorination process, i.e., partial breakage of C-F bonds, which, apparently, occurs mainly in the outer SWCNTs in SWCNT bundles. After the annealing at T_{DF}=420°C defluorination becomes even more evident [Figs. 9(a) and 9(b), curves 5]. Contrary to the absorption spectra, the F 1*s* photoelectron spectrum changes more dynamically. After the 8th annealing, the new structural feature *A`* was still looking like a small bulge on the low-energy side of the main peak *B*; however, immediately after the 9th annealing [Fig. 9(b), curve 6], relative intensities of the two structural features changed dramatically: the *A`* bulge turned into an intense peak having on the high binding energy side a bulge that had been previously peak *B* associated with the new C-F phases. After the 10th annealing this bulge becomes even less intense, and the spectrum exhibits a single peak *A'* with the binding energy of 686 eV and FWHM=2.5 eV [Fig. 9(b), curve 7]; peak *A'* is asymmetric on side of high binding energies. In effect, annealing caused drastic changes in the F 1*s* photoelectron spectrum: peak *B* (687.6 eV, FWHM=2 eV) has disappeared, and new peak *A'* (686 eV, FWHM=2.5 eV) [Fig. 9(b), curve 8] has arisen. Such transformations of the F 1*s* photoelectron spectrum can be easily explained by our hypothesis that the process of F-SWCNT defluorination is accompanied by fluorination of the sample substrate with formation of a new FeF_x phase.

Similarly to the F 1*s* spectrum, C 1*s* photoelectron spectrum undergoes principal changes after the 9th annealing: the features associated with the new C-F phases, namely, A_1, *B* and *C*, are not clearly seen in the spectrum any more. Notice that, contrary to the A_1 and *B* features, feature *C* intensity remains almost the same. This observation supports the idea that band *C* can be best interpreted as the signal from a fluorine-carbon phase with stronger chemical bonds than those in phases 1 and 2. The presence of this phase is also confirmed by the asymmetrical shape of F 1*s* photoelectron spectrum and by the fact that, even after the 12th annealing, initial shape of the C 1*s* spectrum is not restored: C 1*s* peak (FWHM=1.6 eV, *BE*=284.8 eV) becomes evidently broader, which points to surface deformations of the outer tubes in the bundles.

6. Conclusion

The goal of this work was to study electronic structure of fluorinated single-walled and multi-walled carbon nanotubes. High energy resolution X-ray C 1*s* and F 1*s* absorption and photoelectron spectra of F-SWCNTs with different fluorine contents (35 and 40%) and F-MWCNTs with fluorine contents (10-55%) were measured. By comparing fine structures of F-SWCNTs and F-MWCNTs absorption spectra with HOPG, WGF and nanodiamond spectra we have found out that fluorination processes in single- and multi-walled carbon nanotubes are partly similar. Fluorine atoms interact with single-walled and multi-walled carbon nanotubes by getting covalently attached to $\pi 2p_z$ orbitals of the carbon atoms similar to WGF. It was found out that SWCNTs and MWCNTs cannot be completely fluorinated at the given fluorination temperatures (190-222 °C and 420 °C, respectively). The NEXAFS measurements demonstrated that within the probing depth (~15 nm) of F-MWCNTs, the process of fluorination occurs uniformly and does not depend on the fluorine concentration. Our experimental data confirm the previously predicted possibility of existence of two fluorine super-lattices on the F-CNTs lateral surface, which results in developing of fluorine-carbon phases with C_2F and C_4F stoichiometries. Phase 1 (C_2F) content in F-SWCNTs and F-MWCNTs does not change with the increase in probing depth. It was assumed that phase 2 (C_4F) whose electron transfer is smaller than that in phase 1 is formed only on the SWCNTs located in the near-surface layer of the bundles and at the surface of the F-MWCNTs (1-2 monolayers). At the same time, only in the case of F-SWCNTs, phase 3 (CF) exists. It is characterized by greater electron transfer than phase 1. Probably, phase 3 arises due to fluorine atoms attachment to carbon atoms located at the open edges of SWCNTs. We have revealed that at the temperatures of 190 °C and 222 °C the bundles of single-walled nanotubes are not completely fluorinated within the probing depth of 15-20 nm. The process of F-SWCNT and F-MWCNT defluorination by thermal annealing has been investigated. Defluorination temperatures of F-SWCNTs and F-MWCNTs have been found to be equal to each other and to the F-MWCNTs fluorination temperature (T_{DF} = T_F = 420 °C). We have shown that thermal defluorination of F-SWCNTs contrary to F-MWCNTs is impossible without partial deformation of graphene mesh of F-SWCNTs located on the bundle surface.

Acknowledgments

This work was performed within the scope of the “Russian–German Laboratory at BESSY” bilateral Program and supported by the Russian Foundation for Basic Research (Project No. 09-02-01278).

We thank Dr. Muradyan V.E. and Dr. Shul`ga Yu.M. (Institute of Problems of Chemical Physics, the Russian Academy of Sciences, Chernogolovka, Russia) for samples of F-MWCNTs and the Dr. Krestinin A.V., Zvereva G.I. and Dr. Kharitonov A.P. (Institute of Problems of Chemical Physics, the Russian Academy of Sciences, Chernogolovka, Russia) for samples of F-SWCNTs.

7. References

An, K.H.; Heo, J.G.; Jeon, K.G.; Bae, D.J.; Jo, C.; Yang, C.W.; Park, C.-Y.; Lee, Y.H.; Lee, Y.S. & Chung, Y.S. (2002). X-ray photoemission spectroscopy study of fluorinated single-walled carbon nanotubes. *Appl. Phys. Lett*, Vol. 80, No 22 (June 2002) pp. 4235, ISSN 1077-3118

Banerjee, S.; Hemraj-Benny, T.; Balasubramanian, M.; Fisher, D.A.; Misewich, J.A. & Wong, S.S. (2004). Ozonized single-walled carbon nanotubes investigated using NEXAFS spectroscopy. *Chem. Commun.*, No. 7, (2004) pp. 772-773, ISSN 1359-7345

Banerjee, S.; Hemraj-Benny, T.; Sambasivan, S.; Fischer, D.A.; Misewich, J.A. & Wong, S.S. (2005). Near-edge x-ray absorption fine structure investigations of order in carbon nanotube-based systems. *J. Phys. Chem. B*, Vol. 109, No. 17 (February 2005) pp. 8489-8495, ISSN 1520-6106

Bettinger, H.F.; Kudin, K.N. & Scuseria, G.E. (2001). Thermochemistry of fluorinated single wall carbon nanotubes. *J. Am. Chem. Soc.* Vol. 123, No. 51, (December 2001) pp. 12849-12856, ISSN 0002-7863

Brown, F.C.; Bachrach, R.Y. & Bianconi, A. (1978). Fine structure above the carbon K-edge in methane and in the fluoromethanes. *Chem. Phys. Lett*, Vol. 54, No. 3, (March 1978) pp. 425-429, ISSN 0009-2614

Brzhezinskaya, M.M.; Vinogradov, N.A.; Muradyan, V.E.; Shulga, Yu.M.; Polyakova, N.V. & Vinogradov, A.S. (2008). Characterization of fluorinated multiwalled carbon nanotubes by x-ray absorption spectroscopy. *Phys. Solid State*, Vol. 50, No. 3 (March 2008) pp. 587-594, ISSN 1063-7834

Brzhezinskaya, M.M.; Vinogradov, N.A.; Muradyan, V.E.; Shul'ga, Yu.M.; Puettner, R.; Vinogradov, A.S. & Gudat, W. (2009, a). Specific features of the electronic structure of fluorinated multiwalled carbon nanotubes in the near-surface region. *Phys. Solid State*, Vol. 51, No. 9, (September 2009) pp. 1961-1971, ISSN 1063-7834

Brzhezinskaya, M.M.; Muradyan, V.E.; Vinogradov, N.A.; Preobrajenski, A.B.; Gudat, W. & Vinogradov, A.S. Electronic structure of fluorinated multiwalled carbon nanotubes studied using x-ray absorption and photoelectron spectroscopy. *Phys. Rev. B*, Vol. 79, No. 15, (2009, b) pp. 155439(12), ISSN 1098-0121

Brzhezinskaya, M.M.; Vinogradov, A.S.; Krestinin, A.V.; Zvereva, G.I.; Kharitonov, A.P. & Kulakova, I. I. (2010). Characterization of fluorinated singlewalled carbon nanotubes by X-ray absorption spectroscopy. *Phys. Solid State*, Vol. 52, No. 4, (April 2010) (in print), ISSN 1063-7834

Burghard, M. (2005). Electronic and vibrational properties of chemically modified single-wall carbon nanotubes. *Surf. Sci. Rep.*, Vol. 58, Nos. 1-4, (August 2005) pp. 1-109, ISSN 0167-5729

Chen, J.G. (1997). NEXAFS investigations of transition metal oxides, nitrides, carbides, sulfides and other interstitial compounds. *Surf. Sci. Rep.*, Vol. 30, Nos. 1-3, (October 1997) pp. 1-152, ISSN 0167-5729

Dresselhaus, M.S.; Dresselhaus, G. (2001). *Carbon Nanotubes: Synthesis, Structure, Properties and Applications: Topics in Applied Physics*, Springer-Verlag, ISBN 3540410864, Berlin

Ewels, C.P.; Van Lier, G.; Charlier, J.C.; Heggie, M.I. & Briddon, P.R. (2006). Pattern formation on carbon nanotube surfaces. *Phys. Rev. Lett.* Vol. 96, No. 21, (May 2006) pp. 216103(4), ISSN 0031-9007

Fujita, M.; Wakabayashi, K.; Nakada, K. & Kusakabe, K. (1996). Peculiar localized state at zigzag graphite edge. *J. Phys. Soc. Jpn.*, Vol. 65, No. 7, (July 1996) pp. 1920-1923, ISSN 0031-9015

Gudat W. & Kunz, C. (1972). Close Similarity between Photoelectric yield and photoabsorption spectra in the soft-x-ray range. *Phys. Rev. Lett*, Vol. 29, No. 3 (July 1972) pp. 169-172, ISSN 0031-9007

Gupta, V.; Nakajima, T.; Ohzawa, Y. & Zemva, B. 2003. A study on the formation mechanism of graphite fluorides by Raman spectroscopy. *J. Fluorine Chem.,* Vol. 120, No. 2, (April 2003) pp. 143-150, ISSN 0022-1139

Hamwi, A.; Alvergnat, H.; Bonnamy, S. & Béguin, F. (1997). Fluorination of carbon nanotubes. *Carbon*, Vol. 35, No. 6, (May 1997) pp. 723-728, ISSN 0008-6223

Hayashi, T.; Terrones, M.; Scheu, C.; Kim, Y.A.; Rühle, M.; Nakajima, T. & Endo, M. (2002). NanoTeflons: structure and EELS characterization of fluorinated carbon nanotubes and nanofibers. *Nano Lett.*, Vol. 2, No. 5, (May 2002) pp. 491-496, ISSN 1530-6984

Hemraj-Benny, T.; Banerjee, S.; Sambasivan, S.; Fischer, D.A.; Eres, G.; Puretzky, A.A.; Geohegan, D.B.; Lowndes, D.H.; Misewich, J.A. & Wong, S.S. (2006). Imperfect surface order and functionalization in vertical carbon nanotube arrays probed by near edge X-ray absorption fine structure spectroscopy (NEXAFS). Phys. Chem. Chem. Phys., Vol. 8, No. 43, (2006) pp. 5038-5044, ISSN 1463-9076

Hernandez, E.; Goze, C.; Bernier, P. & Rubio, A. (1999). Elastic properties of single-wall nanotubes. *Appl. Phys. A*, Vol. 68, No. 3, (March 1999) pp. 287-292, ISSN 0947-8396

Huefner, S. (2003). *Photoelectron Spectroscopy*, Springer, ISBN 978-3-540-41802-3, Berlin.

Kelly, K.F.; Chiang, I.W.; Mickelson, E.T.; Hauge, R.H.; Margrave, J.L.; Wang, X.; Scuseria, G.E.; Radloff, C. & Halas, N.J. 1999. Insight into the mechanism of sidewall functionalization of single-walled nanotubes: an STM study. *Chem. Phys. Lett*, Vol. 313, Nos 3-4, (November 1999) pp. 445-450, ISSN 0009-2614

Khabashesku, V.N.; Billups, W.E. & Margrave, J.L. (2002). Fluorination of single-wall carbon nanotubes and subsequent derivatization reactions. *Acc. Chem. Res.*, Vol. 35, No. 12, (December 2002) pp. 1087-1095, ISSN 0001-4842

Kiselev, N.A.; Moravsky, A.P.; Ormont, A.B. & Zakharov, D.N. (1999). SEM and HREM study of the internal structure of nanotube rich carbon arc cathodic deposits. *Carbon*, Vol. 37, No. 7, (June 1999) pp. 1093-1103, ISSN 0008-6223

Klein, D.J. 1994. Graphitic polymer strips with edge states. *Chem. Phys. Lett*, Vol. 217, No. 3, (January 1994) pp. 261-265, ISSN 0009-2614

Kobayashi, Y.; Fukui, K.; Enoki, T.; Kusakabe, K. & Kaburagi, Y. 2005. Observation of zigzag and armchair edges of graphite using scanning tunneling microscopy and spectroscopy. *Phys. Rev. B*, Vol. 71, No. 19 (May 2005) pp. 193406(4), ISSN 1098-0121

Krestinin, A.V.; Kiselev, N.A.; Raevskii, A.V.; Ryabenko, A.G.; Zakharov, D.N. & Zvereva, G.I. (2003, a). Perspectives of single-wall carbon nanotube production in the arc discharge process. *Eurasian Chem. Tech. J.*, Vol. 5, No. 1, (January 2003) pp. 7-18, ISSN 1562-3920

Krestinin, A.V.; Raevskii, A.V.; Kiselev, N.A.; Zvereva, G.I.; Zhigalina, O.M. & Kolesova, O.I. (2003, b). Optical activity effect in crystalline structures of purified single-wall carbon nanotubes. *Chem. Phys. Lett*, Vol. 381, Nos. 5-6, (November 2003) pp. 529-534, ISSN 0009-2614

Krestinin, A.V.; Kharitonov, A.P.; Shul'ga, Yu.M.; Gigalina, O.M.; Knerelman, E.I.; Brzhezinskaya, M.M.; Vinogradov, A.S.; Preobrajenski, A.B.; Zvereva, G.I.; Kislov, M.B.; Martinenko, V.M.; Korobov, I.I.; Davidova, G.I.; Gigalina, V.G. & Kiselev, N.A. 2009. The synthesis and characterization of fluorinated single-walled carbon nanotubes. *Nanotechnologies in Russia*, Vol. 4, No. 1-2, (January 2009) pp. 60-78, ISSN 1995-0780

Kudin, K.N.; Bettinger, H.F. & Scuseria, G.E. (2001). Fluorinated single-wall carbon nanotubes. *Phys. Rev. B*, Vol. 63, No. 4 (January 2001) pp. 045413(8), ISSN 1098-0121

Kuznetsova, A.; Popova, I.; Yates, J.T.; Bronikowski, M.J.; Huffman, C.B.; Liu, J.; Smalley, R.E.; Hwu, H.H. & Chen, J.G. (2001). Oxygen-containing functional groups on single-wall carbon nanotubes: NEXAFS and vibrational spectroscopic studies. *J. Am. Chem. Soc.* Vol. 123, No. 43, (October 2001) pp. 10699-10704, ISSN 0002-7863

Lebedev, N.G.; Zaporotskova, I.V. & Chernozatonskii, L.A. (2003). Fluorination of carbon nanotubes within the molecular cluster method. *Microelectron. Eng.*, Vol. 69, Nos. 2-4, (September 2003) p. 511-518, ISSN 0167-9317

Lee, Y.S.; Cho, T.H.; Lee, B.K.; Rho, J.S.; An, K.H. & Lee, Y.H. J. (2003). Surface properties of fluorinated single-walled carbon nanotubes. *J. Fluorine Chem..*, Vol. 120, No. 2, (April 2003) p. 99-104, ISSN 0022-1139

Lee, Y.-S. (2007). Syntheses and properties of fluorinated carbon materials. *J. Fluorine Chem.*, Vol. 128, No. 4, (April 2007) pp. 392-403, ISSN 0022-1139

Louie, S.G. (2001). Electronic properties and defects, In: *Carbon Nanotubes*, Dresselhaus, M.S.; Dresselhaus, G. & Avouris, Ph., (Eds.), pp. 117-152, Springer-Verlag, ISBN 978-3-540-41086-7, Berlin

Martin, C.; Arakawa, E.T.; Callcott, T.A. & Ashley, J.C. (1985). Low energy electron attenuation length studies in thin amorphous carbon films. *J. Electron Spectrosc. Relat. Phenom.* Vol. 35, No. 2, (March 1985) pp. 307-317, ISSN 0368-2048

Maruyama, M.; Kusakabe, K.; Tsuneyuki, S.; Akagi, K.; Yoshimoto, Y. & Yamauchi, J. 2004. Magnetic properties of nanographite with modified zigzag edges. *J. Phys. Chem. Solids*, Vol. 65, Nos. 2-3, pp. 119-122 (March 2004), ISSN 0022-3697

Mickelson, E.T.; Huffman, C.B.; Rinzler, A.G.; Smalley, R.E.; Hauge, R.H. & Margrave, J.L. (1998). Fluorination of single-wall carbon nanotubes. *Chem. Phys. Lett*, Vol. 296, Nos. 1-2, (October 1998) pp. 188-194, ISSN 0009-2614

Mickelson, E.T.; Chiang, I.W.; Zimmerman, J.L.; Boul, P.J.; Lozano, J.; Liu, J.; Smalley, R.F.; Hauge, R.H. & Margrave, J.L. (1999). Solvation of fluorinated single-wall carbon nanotubes in alcohol solvents. *J. Phys. Chem. B.* Vol. 103, No. 21 (May 1999) pp. 4318-4322, ISSN 1520-6106

Mitmire, J.W. & White, C.T. (1997). In: *Carbon nanotubes*. Ebbesen, T.W. (Ed.), pp. 191-224, CRC Press, ISBN 0849396026, Boca Raton, FL

Molodtsov, S.L.; Fedoseenko, S.I.; Vyalikh, D.V.; Iossifov, I.E.; Follath, R.; Gorovikov, S.A.; Brzhezinskaya, M.M.; Dedkov, Yu.S.; Puettner, R.; Schmidt, J.-S.; Adamchuk, V.K.; Gudat, W. & Kaindl, G. (2009). High-resolution Russian–German beamline at BESSY. *Appl. Phys. A*, Vol. 94, No. 3, (March 2009) pp. 501-505, ISSN 0947-8396

Okotrub, A.V.; Yudanov, N.F.; Chuvilin, A.L.; Asanov, I.P.; Shubin, Yu.V.; Bulusheva, L.G.; Gusel'nikov, A.V. & Fyodorov, I.S. (2000). Fluorinated cage multiwall carbon nanoparticles. *Chem. Phys. Lett*, Vol. 322, Nos. 3-4 (May 2000) pp. 231-236, ISSN 0009-2614

Park, K.A.; Choi, Y.S.; Lee, Y.H. & Kim, C. (2003). Atomic and electronic structures of fluorinated single-walled carbon nanotubes. *Phys. Rev. B*, Vol. 68, No. 4 (July 2003) pp. 045429(8), ISSN 1098-0121

Rosenberg, R.A.; Love, P.J. & Rehn, V. 1986. Polarization-dependent C(*K*) near-edge x-ray-absorption fine structure of graphite. *Phys. Rev. B*, Vol. 33, No. 6 (March 1986) pp. 4034-4037, ISSN 1098-0121

Saito, R.; Yagi, M.; Kimura, T.; Dresselhaus, G. & Dresselhaus, M.S. 1999. Electronic structure of fluorine doped graphite nanoclusters. *J. Phys. Chem. Solids*, Vol. 60, No. 6, (June 1999) pp. 715-721, ISSN 0022-3697

Sato, Y.; Hagiwara, R. & Ito, Y. 2003. Refluorination of pyrocarbon prepared from fluorine–GIC. *Solid State Sci.*, Vol. 5, No. 9, (September 2003) pp. 1285-1290, ISSN 1293-2558

Schiessling, J.; Kjeldgaard, L.; Rohmund, F.; Falk, L.K.L.; Campbell, E.E.B.; Nordgren, J. & Brühwiler, P.A. (2003). Synchrotron radiation study of the electronic structure of multiwalled carbon nanotubes. *J. Phys.: Condens. Matter*, Vol. 15, No. 38, (October 2003) pp. 6563-6579, ISSN 0953-8984

Seifert, G.; Kohler, T. & Frauenheim, T. 2000. Molecular wires, solenoids, and capacitors by sidewall functionalization of carbon nanotubes. *Appl. Phys. Lett*, Vol. 77, No 9, (August 2000) pp. 1313(3), ISSN 1077-3118

Stöhr, J. (2003). *NEXAFS Spectroscopy*, Springer, ISBN-13 978-3540544227, Berlin

Shul'ga, Y.M.; Tien, T.-C.; Huang, C.-C.; Lo, S.-C.; Muradyan, V.E.; Polyakova, N.V.; Ling, Y.-C.; Loufty, R.O. & Moravsky, A.P. (2007). XPS study of fluorinated carbon multi-walled nanotubes. *J. Electron Spectrosc. Relat. Phenom.*, Vol. 160, Nos. 1-3, (August 2007) pp. 22-28, ISSN 0368-2048

Tang, Y.H.; Sham, T.K.; Hu, Y.F.; Lee, C.S. & Lee, S.T. (2002). Near-edge X-ray absorption fine structure study of helicity and defects in carbon nanotubes. *Chem. Phys. Lett*, Vol. 366, Nos. 5-6, (December 2002) pp. 636-641, ISSN 0009-2614

Touhara, H. & Okino, F. (2000). Property control of carbon materials by fluorination. *Carbon*, Vol. 38, No. 2, (December 2000) pp. 241-267, ISSN 0008-6223

Van Lier, G. ; Ewels, C.P.; Zuliani, F. ; De Vita, A. & Charlier, J.-C. (2005). Theoretical analysis of fluorine addition to single-walled carbon nanotubes: functionalization routes and addition patterns. *J. Phys. Chem. B*, Vol. 109, No. 13, (March 2005) pp. 6153-6158, ISSN 1520-6106

Vinogradov, A.S.; Fedoseenko, S.I.; Krasnikov, S.A.; Preobrajenski, A.B.; Sivkov, V.N.; Vyalikh, D.V.; Molodtsov, S.L.; Adamchuk, V.K.; Laubschat, C. & Kaindl G. 2005. Low-lying unoccupied electronic states in 3*d* transition-metal fluorides probed by NEXAFS at the F 1*s* threshold. *Phys. Rev. B*, Vol. 71, No. 4 (January 2005) pp. 045127(11), ISSN 1098-0121

Yudanov, N.F.; Okotrub, A.V.; Shubin, Yu.V.; Yudanova, L.I.; Bulusheva, L.G.; Chuvilin, A.L. & Bonard, J.-M. (2002). Fluorination of arc-produced carbon material containing multiwall nanotubes. *Chem. Mater.*, Vol. 14, No. 4, (April 2002) pp. 1472-1476, ISSN 0897-4756

Zhou, J.; Zhou, X.; Sun, X.; Li, R.; Murphy, M.; Ding, Z.; Sun, X. & Sham, T.-K. (2007). Interaction between Pt nanoparticles and carbon nanotubes – An X-ray absorption near edge structures (XANES) study. *Chem. Phys. Lett*, Vol. 437, Nos. 4-6 (April 2007) pp. 229-232, ISSN 0009-2614

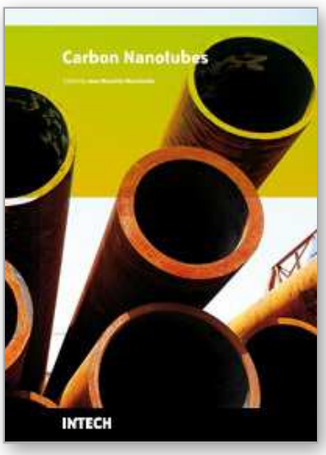

Carbon Nanotubes

Edited by Jose Mauricio Marulanda

ISBN 978-953-307-054-4
Hard cover, 766 pages
Publisher InTech
Published online 01, March, 2010
Published in print edition March, 2010

This book has been outlined as follows: A review on the literature and increasing research interests in the field of carbon nanotubes. Fabrication techniques followed by an analysis on the physical properties of carbon nanotubes. The device physics of implemented carbon nanotubes applications along with proposed models in an effort to describe their behavior in circuits and interconnects. And ultimately, the book pursues a significant amount of work in applications of carbon nanotubes in sensors, nanoparticles and nanostructures, and biotechnology. Readers of this book should have a strong background on physical electronics and semiconductor device physics. Philanthropists and readers with strong background in quantum transport physics and semiconductors materials could definitely benefit from the results presented in the chapters of this book. Especially, those with research interests in the areas of nanoparticles and nanotechnology.

INTECH
open science | open minds

InTech Europe
University Campus STeP Ri
Slavka Krautzeka 83/A
51000 Rijeka, Croatia
Phone: +385 (51) 770 447
Fax: +385 (51) 686 166
www.intechopen.com

InTech China
Unit 405, Office Block, Hotel Equatorial Shanghai
No.65, Yan An Road (West), Shanghai, 200040, China
中国上海市延安西路65号上海国际贵都大饭店办公楼405单元
Phone: +86-21-62489820
Fax: +86-21-62489821

IntechOpen